# Dynamic Output-Feedback Decentralized Control Synthesis for Integration of Distributed Energy Resources in AC Microgrids

Ricardo Pérez-Ibacache, Rafael S. Castro, Guilherme Araujo Pimentel, and Bruno Salgado Bizzo

***Abstract*—This work proposes a control design procedure based on Linear Matrix Inequalities (LMI) for integrating Distributed Energy Resources (DERs) in microgrid systems. Each DER uses local measurements as feedback, so this proposal results in a method to design a decentralized primary control. The dynamic model employed to synthesize such a controller presents an unmeasured state vector, model uncertainties, and random disturbances. To simultaneously deal with all these difficulties while ensuring the closed-loop stability and multiple performance specifications, this work is formulated in terms of a single Lyapunov function. To find this Lyapunov function and synthesize the controller gains, a convex optimization problem that involves LMIs is required to be solved. The controller results in a linear discrete-time output-feedback form, facilitating its implementation. The time-domain simulation of a microgrid system is performed in the software PSCAD/EMTDC with four DERs to validate the control design procedure's effectiveness.**

***Index Terms*—Linear matrix inequalities, multivariable robust control, primary control of microgrids, voltage and frequency regulation.**

## I. Introduction

DISTRIBUTED Energy Resources (DERs) are essential elements to improve modern electrical power systems' resilience and energy efficiency. However, as the number of disruptive events in the power network increases, the deployment of DER units within microgrids is compelled to satisfy energy quality standards and, most importantly, to guarantee stability [1]–[3]. The mechanism responsible for stabilizing the microgrid system is the so-called primary control, which corresponds to a feedback law based only on local or decentralized measurements. The challenge of designing such a controller arises from the fact that the microgrid model is mainly subject to random unmeasured disturbances and model uncertainties, e.g., topological changes, unbalanced and non-linear loads, high-frequency pulse-width voltage modulation, and transition between modes of operation [2], [3].

In recent years, relevant contributions have determined the consequences of the droop-based primary controllers on the stability of islanded microgrids [4]–[6]. However, as the low and medium voltage distribution networks are significantly resistive, the active and reactive powers present a degree of coupling with the voltage and load angle that can not be disregarded. As a possible remedy to this degree of coupling, combined primary and secondary controllers (distributed or centralized) have also called the attention of the scientific community [7]–[9]. However, as a centralized or distributed control structure relies on the communication infrastructure, the microgrid's stability may be compromised. Hence, the current publication center the attention on decentralized microgrid robust control design. One of the widely used mechanisms to achieve orientation and synchronization in decentralized microgrids is the phase-lock-loop (PLL) algorithm; however, according to [3], those control approaches exhibit low stability and performance robustness when the microgrid operates in islanded mode. This limitation arises from the complexity of an islanded microgrid itself, where the dynamic response of the voltage and frequency are in the same time order of the PLL response, jeopardizing the decoupling assumption made in grid-connected mode [10]. Therefore, those control approaches based on PLL are disregarded from the discussion in this work. Hence, under these arguments, the control problem can then be formulated by considering a single model that brings together all the involved variables in the same framework, including the orientation of the system model with a specific reference frame and the synchronization process among DER units, as discussed by [11]–[14]. The central aspect of considering a model that characterizes all the electrical dynamics is that a dynamical output-feedback controller is required to be synthesized while desired performance specifications are satisfied. In [15], for time-invariant linear systems, these challenges are addressed by formulating a convex optimization problem that satisfies the Lyapunov stability conditions and that can be solved using standard software packages. In a previous author's work [13], a dynamic output-feedback controller based on the linear-quadratic-gaussian/loop-transfer-recovery (LQG/LTR) procedure was proposed for a reduced model in the context of microgrids. This procedure only considers the

Manuscript received December 14, 2020; revised April 7, 2021 and August 7, 2021; accepted October 17, 2021. Date of publication November 2, 2021; date of current version February 21, 2022. This work was supported by the Coordenação de Aperfeiçoamento de Pessoal de Nível Superior (CAPES), Brazil—Finance Code 001. Paper no. TSG-01859-2020. *(Corresponding author: Ricardo Pérez-Ibacache.)*

Ricardo Pérez-Ibacache is with the Department of Engineering, Andes Volt Industrial, Valdivia 5090000, Chile (e-mail: rperez@unmanned.cl).

Rafael S. Castro and Bruno Salgado Bizzo are with the School of Technology, Pontifical Catholic University of Rio Grande do Sul, Porto Alegre 90619-900, Brazil (e-mail: rafael.castro@pucrs.br; bruno.bizzo@edu.pucrs.br).

Guilherme Araujo Pimentel is with the Systems, Estimation, Control and Optimization Group, University of Mons, 7000 Mons, Belgium (e-mail: guilherme.araujopimentel@umons.ac.be).

Color versions of one or more figures in this article are available at https://doi.org/10.1109/TSG.2021.3124859.

Digital Object Identifier 10.1109/TSG.2021.3124859

separate minimization of two quadratic cost functions (LQE and LQR problems), which, as is discussed in [16], may degrade the closed-loop system performance significantly.

In order to ensure stability and performance robustness in microgrid systems, the primary control design should consider the attenuation of different disturbances perceived by each DER's closed-loop and offer a systematic way to include different performance specifications. In that spirit, this work presents a dynamic model and a multiobjective control design problem that allows us to provide simultaneous closed-loop performance specifications to the primary control design. The analytical results presented in [15] are therefore employed in the current publication to solve the dynamic output-feedback control design problem.

The use of linear matrix inequalities (LMIs) to formulate a multiobjective control synthesis problem has become a standard tool in advanced control design [17]–[19]. It allows us to formulate a mix of time- and frequency-domain specifications by considering a single Lyapunov function, which guarantees closed-loop stability while complying with the desired closed-loop specifications. Once the control synthesis problem is formulated using a semidefinite program involving LMIs, it can be numerically solved with standard optimization algorithms [20]. In the context of DER units within microgrid systems, the use of LMIs for control design purposes has been previously considered in [21]–[28], among others. However, in general, the control strategies assume a PLL algorithm for synchronization and orientation purposes, or they are cascade control structures conceived for a specific mode of operation; islanded or grid-connected. The microgrid system, operating under these considerations, may exhibit low stability and performance robustness [3]. On the other hand, robust control design in the context of microgrids has been emphasized in [29]–[31], where the benefits on the microgrid stability are evidenced. Particularly, the $\mathcal{H}_\infty$-control is proposed to improve the disturbance rejection capability. While the $\mathcal{H}_\infty$ specification enforces robust stability when the system is subject to model uncertainties, as previously reported in [29]–[31], the contribution of the current work is to present a primary control design methodology that allows us to include diverse closed-loop specifications in a single convex optimization problem. Particularly, in this work, the $\mathcal{H}_2$ performance and a minimum exponential decay rate criteria are included to minimize the energy of the controlled variables when the system is subject to pulse disturbances and to provide a proper closed-loop settling time. Furthermore, all the above specifications are normalized for the DER unit's nominal values, obtaining a systematic primary control design procedure that responds proportionally to the DER's nominal power. Finally, the small-gain theorem is employed to quantify the degree of robustness of the resulting controller. Hence, this paper aims to solve the following control problem.

*Problem 1 (DER Unit's Primary Control Design):* Design a dynamic output-feedback primary controller for integration of DER units in microgrid systems such that the closed-loop exhibits $\mathcal{H}_2/\mathcal{H}_\infty$ performance and a minimum closed-loop exponential decay rate.

The notation is standard, the subindex $k \in \mathbb{N}$ is the instant of sampling time, in block matrices, $\star$ is used to denote its symmetric elements, the acronym svd$(\cdot)$ is used to denote the singular value decomposition, Tr corresponds to the trace operator, $\mathbf{0}_{n\times m}$ is a matrix of zeros with $n \times m$ its dimension, and $\mathbf{I}$ is the identity matrix of a proper dimension.

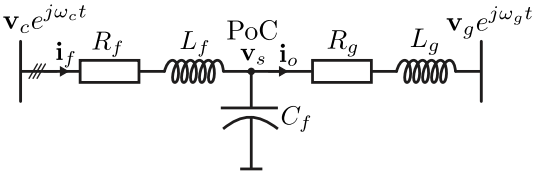


Fig. 1. Lumped circuit representation of the interaction between a DER unit integration and a microgrid.

## II. Preliminaries

This section presents (*i*) the dynamic model that characterizes a DER unit's interaction within a microgrid, (*ii*) the LMI based problem formulation that satisfies multiple closed-loop specification performances, and (*iii*) the small-gain theorem. This publication considers a formulation based on a discrete-time framework.

### A. Full DER-Microgrid Interaction Model

The circuit representation in Fig. 1 characterizes the interaction between a voltage-sourced converter (VSC) and a microgrid in stationary $\alpha\beta$-frame. The VSC is represented by a variable voltage and frequency source, $\mathbf{v}_c e^{j\omega_c t}$, with $\mathbf{v}_c \in \mathbb{C}$ and $\omega_c \in \mathbb{R}$. This VSC is connected through a $L_f C_f$ output filter to the microgrid at its point-of-connection (PoC). The microgrid is represented by a voltage and frequency source $\mathbf{v}_g e^{j\omega_g t}$ in series with a weak link characterized by $L_g R_g$ parameters. In practice, as the output filter is integrated into the DER unit, the parameters $L_f C_f$ are assumed to be known. On the other hand, $R_g L_g$ represents the microgrid's characteristic parameters, which can not be accurately known. Hence, for control synthesis purposes, the DER's isolation transformer's short-circuit parameters are considered as an approximation of the microgrid model [32]. Besides, as $\mathbf{v}_g$ and $\omega_g$ condense all the unmodeled dynamics of the microgrid, they are considered to be energy-bounded signals.

The difficulty of obtaining the dynamic model of an electrical network that includes variable-frequency voltage sources can be overcome using a rotating reference *dq*-frame [32]. Considering that the lumped model that describes the DER-microgrid interaction is expressed in a reference frame that rotates with an arbitrary-frequency $\omega_c$ and an arbitrary-phase, the set of differential equations can be written as

$$\begin{aligned}
\frac{d\mathbf{i}_f}{dt} &= -\frac{R_f}{L_f}\mathbf{i}_f - j\omega_c\mathbf{i}_f - \frac{\mathbf{v}_s}{L_f} + \frac{\mathbf{v}_c}{L_f},\\
\frac{d\mathbf{v}_s}{dt} &= -\frac{\mathbf{i}_o}{C_f} - j\omega_c\mathbf{v}_s + \frac{\mathbf{i}_f}{C_f},\\
\frac{d\mathbf{i}_o}{dt} &= -\frac{R_g}{L_g}\mathbf{i}_o - j\omega_c\mathbf{i}_o - \frac{\mathbf{v}_g}{L_g}e^{j\delta} + \frac{\mathbf{v}_s}{L_g},\\
\frac{d\delta}{dt} &= \omega_g - \omega_c,
\end{aligned} \tag{1}$$

where $\{(\mathbf{i}_f, \mathbf{v}_s, \mathbf{i}_o), \delta\} \in \{\mathbb{C}, \mathbb{R}\}$ are the state variables, $\{\mathbf{v}_c, \omega_c\} \in \{\mathbb{C}, \mathbb{R}\}$ are the control inputs and $\{\mathbf{v}_g, \omega_g\} \in \{\mathbb{C}, \mathbb{R}\}$

are the disturbance inputs. The measured output of this model correspond to the currents $\mathbf{i}_f$, $\mathbf{i}_o$ and to the voltage $\mathbf{v}_s$.

It is worth mentioning that from (1), the dynamic of state variable $\delta$ play a vital role in the control design, as highlighted in [13]. The consequences of this state variable $\delta$ should not be overlooked; it characterizes the frequency difference between the DER unit's frequency $\omega_c$ and the microgrid's frequency $\omega_g$ or, in other words, the synchronization dynamics of the system model. This approach allows us to disregard using a dedicated PLL for synchronization purposes; instead, all the involved dynamics are combined in a single control design framework. As a consequence of including $\delta$ as a state variable in the control design (that is not directly measured), an output-feedback controller is required to be synthesized. Finally, to orientate the system model, and hence the controller, the quadrature axis of the voltage $\mathbf{v}_s$ is regulated to zero though the designed controller, i.e., $v_{sq}^* = 0$; it means that the orientation dynamic is also characterized in the system model for closed-loop design.

This publication deals with a linear time-invariant representation of (1). To that end, the state-space (1) is linearized around the origin of the currents, i.e., $\bar{\mathbf{i}}_f = \bar{\mathbf{i}}_o = 0$, and around the nominal voltage and frequency of the microgrid, i.e., $\{\overline{\mathbf{v}}_g, \overline{\omega}_g\} = \{v_{\mathbf{b}}, \omega_{\mathbf{b}}\}$. Expressing the complex variables in their real components $\{x_d, x_q\}$ (with the complex vector written as $\mathbf{x} = x_d + jx_q$), the linear model can be written as

$$\dot{x} = A_s x + B_s u + B_{ws} w, \tag{2a}$$

$$y = C_s x + D_{ws} w, \tag{2b}$$

where

$$x = \begin{bmatrix} i_{fd} & i_{fq} & v_{sd} & v_{sq} & i_{od} & i_{oq} & \delta \end{bmatrix}^T, \tag{3a}$$

$$u = \begin{bmatrix} v_{cd} & v_{cq} & \omega_c \end{bmatrix}^T, \tag{3b}$$

$$y = \begin{bmatrix} i_{fd} & i_{fq} & v_{sd} & v_{sq} & i_{od} & i_{oq} \end{bmatrix}^T. \tag{3c}$$

In regard of the input disturbance $w$, it is considered that, in addition to the disturbances identified at the grid model, represented by $w_g = [\, v_{gd} \;\; v_{gq} \;\; \omega_g \,]^T$, other two input disturbances signals are considered to include further performance specifications. These additional disturbances are modeled at the input and at the measured output of the model and are represented by $w_u \in \mathbb{R}^3$ and $w_y \in \mathbb{R}^6$, respectively. Hence, the disturbance vector is written as,

$$w = \left[\, w_g^T \;\vdots\; w_u^T \;\vdots\; w_y^T \,\right]^T. \tag{4}$$

Finally, the matrices in (2a) are defined as,

$$A_s = \begin{pmatrix} -\frac{R_f}{L_f} & \omega_{\mathbf{b}} & -\frac{1}{L_f} & 0 & 0 & 0 & 0 \\ -\omega_{\mathbf{b}} & -\frac{R_f}{L_f} & 0 & -\frac{1}{L_f} & 0 & 0 & 0 \\ \frac{1}{C_f} & 0 & 0 & \omega_{\mathbf{b}} & -\frac{1}{C_f} & 0 & 0 \\ 0 & \frac{1}{C_f} & -\omega_{\mathbf{b}} & 0 & 0 & -\frac{1}{C_f} & 0 \\ 0 & 0 & \frac{1}{L_g} & 0 & -\frac{R_g}{L_g} & \omega_{\mathbf{b}} & 0 \\ 0 & 0 & 0 & \frac{1}{L_g} & -\omega_{\mathbf{b}} & -\frac{R_g}{L_g} & -\frac{v_{\mathbf{b}}}{L_g} \\ 0 & 0 & 0 & 0 & 0 & 0 & 0 \end{pmatrix}, \tag{5}$$

$$B_s = \begin{pmatrix} \frac{1}{L_f} & 0 & 0 \\ 0 & \frac{1}{L_f} & 0 \\ & \mathbf{0}_{4\times 3} & \\ 0 & 0 & -1 \end{pmatrix}, \; B_{ws} = \left(\begin{array}{ccc:c:c} & \mathbf{0}_{4\times 3} & & & \\ \frac{-1}{L_g} & 0 & 0 & B_s & \mathbf{0}_{7\times 6} \\ 0 & \frac{-1}{L_g} & 0 & & \\ 0 & 0 & 1 & & \end{array}\right), \tag{6}$$

and the matrices in (2b) as

$$C_s = \begin{pmatrix} \mathbf{I}_6 & \mathbf{0}_{6\times 1} \end{pmatrix}, \quad D_{ws} = \begin{pmatrix} \mathbf{0}_{6\times 3} & \mathbf{0}_{6\times 3} & \mathbf{I}_6 \end{pmatrix}. \tag{7}$$

As aforementioned, the control synthesis is carried out for a discrete-time model of (2) with sampling time $\Delta$. Thus, considering that the input and the disturbance vectors remain constant between sampling time, the zero-order hold discretization method is applied to obtain the next discrete-time model [33],

$$\left[\begin{array}{c:c:c} A & B & B_w \\ \hdashline \mathbf{0} & \mathbf{I} & \mathbf{0} \\ \hdashline \mathbf{0} & \mathbf{0} & \mathbf{I} \end{array}\right] = e^{M_s \Delta} \quad \text{with} \quad M_s = \left[\begin{array}{c:c:c} A_s & B_s & B_{ws} \\ \hdashline \mathbf{0} & \mathbf{0} & \mathbf{0} \\ \hdashline \mathbf{0} & \mathbf{0} & \mathbf{0} \end{array}\right] \tag{8}$$

$$C = C_s, \quad D_w = D_{ws}. \tag{9}$$

Next, a brief discussion on Lyapunov-based control design methodology that is subject to LMIs is presented.

### *B. Dynamic Output-Feedback Synthesis Based on LMI*

As described in the Problem 1, the integration of DER units in microgrid systems should satisfy individual closed-loop specifications; in particular, $\mathcal{H}_2$, $\mathcal{H}_\infty$, and minimum exponential decay rate. These specifications can be formulated in a single convex optimization problem that involves LMIs, offering a systematic procedure to solve a multiobjective control synthesis problem. In this work, the control synthesis is carried out by considering a linear discrete time-invariant representation of the plant as:

$$\begin{aligned} x_{k+1} &= Ax_k + Bu_k + B_w w_k, \\ y_k &= Cx_k + D_w w_k, \\ z_k &= C_z x_k + D_z u_k + D_{zw} w_k \end{aligned} \tag{10}$$

where $x_k \in \mathbb{R}^{n_x}$, $u_k \in \mathbb{R}^{n_u}$ and $y_k \in \mathbb{R}^{n_y}$ are the state, the input, and the measured output, respectively; $w_k \in \mathbb{R}^{n_w}$ represents a vector of exogenous inputs, and $z_k \in \mathbb{R}^{n_z}$ represents the output signal associated to the closed-loop performance. This nominal representation of the system is used for the synthesis of a dynamic output-feedback controller

$$\begin{aligned} \zeta_{k+1} &= A_c \zeta_k + B_c y_k, \\ u_k &= C_c \zeta_k + D_c y_k \end{aligned} \tag{11}$$

where $\zeta \in \mathbb{R}^{n_\zeta}$. Combining the system model (10) and the controller (11), the closed-loop system in its state-space representation can be written as

$$\begin{aligned} \mathcal{X}_{k+1} &= \mathcal{A}\mathcal{X}_k + \mathcal{B} w_k, \\ z_k &= \mathcal{C}\mathcal{X}_k + \mathcal{D} w_k, \end{aligned} \tag{12}$$

with,

$$\left(\begin{array}{c:c} \mathcal{A} & \mathcal{B} \\ \hdashline \mathcal{C} & \mathcal{D} \end{array}\right) = \left(\begin{array}{cc:c} A + BD_cC & BC_c & B_w + BD_cD_w \\ B_cC & A_c & B_cD_w \\ \hdashline C_z + D_zD_cC & D_zC_c & D_{zw} + D_zD_cD_w \end{array}\right) \tag{13}$$

When the closed-loop system requires to be designed to meet multiple performance specifications, one should distinguish, from the closed-loop, the specific disturbances to output channels under design; in this work, the term *realization* is used to refer to these performance channels. Hence, one can specify the $j$-th realization by performing the change of variable $w_k = R_j w_k^{(j)}$ and $z_k^{(j)} = L_j z_k$, where $R_j$ and $L_j$ are chosen based on the desired closed-loop specifications. It yields us to the next closed-loop representation,

$$\begin{aligned} \mathcal{X}_{k+1} &= \mathcal{A}\mathcal{X}_k + \mathcal{B}_j w_k^{(j)}, \\ z_k^{(j)} &= \mathcal{C}_j \mathcal{X}_k + \mathcal{D}_j w_k^{(j)}, \end{aligned} \tag{14}$$

with,

$$\left(\begin{array}{c|c} \mathcal{A} & \mathcal{B}_j \\ \hline \mathcal{C}_j & \mathcal{D}_j \end{array}\right) = \left(\begin{array}{cc|c} A + BD_cC & BC_c & B_j + BD_cF_j \\ B_cC & A_c & B_cF_j \\ \hline C_j + E_jD_cC & E_jC_c & D_j + E_jD_cF_j \end{array}\right) \tag{15}$$

and $B_j = B_w R_j$, $C_j = L_j C_z$, $D_j = L_j D_{zw} R_j$, $E_j = L_j D_z$, $F_j = D_w R_j$.

The control design formulation assumes a stabilizable and detectable closed-loop that admits a quadratic Lyapunov function

$$V(\mathcal{X}_k) = \mathcal{X}_k^T \mathcal{P} \mathcal{X}_k, \quad \mathcal{P} \succ 0 \tag{16}$$

such that

$$\mathcal{A}^T \mathcal{P} \mathcal{A} - \mathcal{P} \prec 0, \tag{17}$$

in order to ensure that $V(\mathcal{X}_{k+1}) - V(\mathcal{X}_k) < 0 \ \forall \mathcal{X}_k \neq 0$. The LMI approach consists of expressing the desired closed-loop performance specifications as additional constraints that satisfy (16) and (17). It results in a nonconvex optimization problem with respect to the controller parameters in (11). The difficulty of finding the controller (11) rises from the nonlinear mapping of the nominal system model and the controller to the closed-loop representation, as seen in (14). In [15], [34], nonetheless, a suitable change of variable was proposed to recover the convexity of the control design problem. This change of variable consists of expressing the Lyapunov matrix $\mathcal{P}$ as,

$$\mathcal{P} = \Pi_2 \Pi_1^{-1}, \tag{18}$$

with

$$\Pi_1 = \begin{pmatrix} \mathbf{X} & \mathbf{I} \\ M^T & \mathbf{0} \end{pmatrix}, \quad \Pi_2 = \begin{pmatrix} \mathbf{I} & \mathbf{Y} \\ \mathbf{0} & N^T \end{pmatrix}, \tag{19}$$

with $\mathbf{X}$ and $\mathbf{Y}$ are symmetric matrices of dimension $n_x$. It means that the dimension of the controller is equal to the system model dimension, $n_\zeta = n_x$, avoiding results with non-strict LMIs [15]. After some analytical manipulation evaluating (18) in (16) and (17), the next change of variable can be found,

$$\begin{aligned} \mathbf{A} &= NA_cM^T + NB_cC\mathbf{X} + \mathbf{Y}BC_cM^T + \mathbf{Y}(A + BD_cC)\mathbf{X}, \\ \mathbf{B} &= NB_c + \mathbf{Y}BD_c, \\ \mathbf{C} &= C_cM^T + D_cC\mathbf{X}, \\ \mathbf{D} &= D_c. \end{aligned} \tag{20}$$

It transforms the control design formulation based on LMI from a nonconvex to a convex optimization problem in the new variables $\{\mathbf{A}, \mathbf{B}, \mathbf{C}, \mathbf{D}\}$. It allows to solve a dynamic output-feedback design problem by exploting standard convex optimization solvers. To solve the optimization problem, one should assume that there exist the decision variables $\mathbf{X} = \mathbf{X}^T \in \mathbb{R}^{n_x \times n_x}$, $\mathbf{Y} = \mathbf{Y}^T \in \mathbb{R}^{n_x \times n_x}$, $\mathbf{A} \in \mathbb{R}^{n_x \times n_x}$, $\mathbf{B} \in \mathbb{R}^{n_x \times n_y}$, $\mathbf{C} \in \mathbb{R}^{n_u \times n_x}$ and $\mathbf{D} \in \mathbb{R}^{n_u \times n_y}$. Once the optimizer finds the numerical values of these decision variables, the controller matrices $\{A_c, B_c, C_c, D_c\}$ can be recovered from transformation (20) through the next algebraic expression

$$\begin{aligned} D_c &= \mathbf{D}, \\ C_c &= (\mathbf{C} - D_cC\mathbf{X})M^{-T}, \\ B_c &= N^{-1}(\mathbf{B} - \mathbf{Y}BD_c), \\ A_c &= N^{-1}\big(\mathbf{A} - NB_cC\mathbf{X} - \mathbf{Y}BC_cM^T - \mathbf{Y}(A + BD_cC)\mathbf{X}\big)M^{-T}, \end{aligned} \tag{21}$$

with $M, N \in \mathbb{R}^{n_x \times n_x}$ are non-singular solutions of $MN^T = \mathbf{I} - \mathbf{X}\mathbf{Y}$. In this work, the matrices $\{M, N\}$ are chosen such that $MN^T = U\Sigma^{\frac{1}{2}}\Sigma^{\frac{1}{2}}V^T = \text{svd}(\mathbf{I} - \mathbf{X}\mathbf{Y})$. One of the key benefits of the LMI formulation is that the closed-loop system satisfies the Lyapunov stability conditions. The sufficiency of the closed-loop system robustness by including these conditions can be explored through the small-gain theorem as presented next.

### C. Small-Gain Theorem

The small-gain theorem accounts for the stability of interconnected systems, where the output of one of them acts as a disturbance to the other. In particular, the theorem is concerned with the input-output stability condition of both systems' feedback connections.

*Assumption 1:* Consider two systems $H_1 : \ell_2 \to \ell_2$ and $H_2 : \ell_2 \to \ell_2$, assume both systems are finite-gain $\ell_2$ stable, that is

$$||y_1||_2 \leq \gamma_1 ||d_1||_2, \forall d_1 \in \ell_2, \tag{22}$$

$$||y_2||_2 \leq \gamma_2 ||d_2||_2, \forall d_2 \in \ell_2, \tag{23}$$

where $d_1$ and $d_2$ represent the disturbances that act on the $H_1$ and $H_2$ systems respectively, and results from the response of the system interconnection of $H_1$ and $H_2$. Let us also assume that the feedback system embedded in each system $H_1$ and $H_2$ is well defined for the complete state-space.

Then, we can say that the feedback connection is finite-gain $\ell_2$ stable if either mapping is finite-gain $\ell$ stable. The small-gain theorem gives sufficient conditions for the finite-gain $\ell$ stability of the feedback connection.

*Theorem 1 (Small-Gain Theorem [35]):* Under the proceeding assumption, the feedback connection is finite-gain stable if $\gamma_1\gamma_2 < 1$.

The above theorem indicates that computing the value of the $\ell_2$ gain of either system, let us say $\gamma_1$, one can find the bounded value of $\gamma_2$ such that the stability condition of the small-gain theorem is satisfied.

In the next section, the LMIs associated with the $\mathcal{H}_2$, $\mathcal{H}_\infty$, and closed-loop exponential decay rate specifications are presented in its discrete-time version for the DER-microgrid integration problem.

## III. Proposed Control Synthesis Specifications for DER Units' Integration in AC Microgrids

This section defines the different input disturbance $w^{(j)}$ to output $z^{(j)}$ channels and their respective $j$-th performance criteria to be satisfied in the control design optimization problem. To that end, let us assume that the output performance signal $z_k$ corresponds to the voltages at the DER unit's PoC and the frequency at the VSC, resulting in the following definition of the signal $z_k$,

$$z_k = \begin{pmatrix} v_{sd} & v_{sq} & \omega_c \end{pmatrix}^T. \tag{24}$$

Hence, considering the definition of the system model matrices in (9) and the output performance signal $z_k$, the definition of the plant model (10) is completed with the next definition,

$$C_z = \left(\begin{array}{c|c|c} \mathbf{0}_{2\times 2} & \mathbf{I}_2 & \mathbf{0}_{2\times 3} \\ \hline \mathbf{0}_{1\times 2} & \mathbf{0}_{1\times 2} & \mathbf{0}_{1\times 3} \end{array}\right), \quad D_z = \left(\begin{array}{c|c} \mathbf{0}_{2\times 2} & \mathbf{0}_{2\times 1} \\ \hline \mathbf{0}_{1\times 2} & 1 \end{array}\right),$$
$$D_{zw} = \left(\begin{array}{c|c|c} \mathbf{0}_{2\times 8} & \mathbf{I}_2 & \mathbf{0}_{2\times 2} \\ \hline \mathbf{0}_{1\times 8} & \mathbf{0}_{1\times 2} & \mathbf{0}_{1\times 2} \end{array}\right). \tag{25}$$

For the controller's synthesis in (11), this work proposes the following closed-loop performance specifications on the respective input-disturbance to the output channel.

### A. Dealing With Stochastic Aspects and Minimum Energy, $\mathcal{H}_2$ Performance

The minimization of the $\mathcal{H}_2$-norm of the closed-loop is equivalent to minimizing the energy and the expected power of the discrete-time output signal $z_k^{(j)}$ ($\ell_2$-norm) when the system is subject to a pulse and white noise in the input disturbance $w_k^{(j)}$,

$$\underset{\text{s.t. } w_k^{(j)} = w_0^{(j)}\delta_k}{\text{minimize}} \left\| z_k^{(j)} \right\|_{\ell_2}. \tag{26}$$

For these reasons, this performance specification is widely used in practical applications, and in this work, it is implemented for the integration of VSC in microgrid systems. This performance specification can be expressed through LMIs, as is presented in the following Proposition.

*Proposition 1 ($\mathcal{H}_2$ Synthesis [15], [19]):* To minimize the $\mathcal{H}_2$ performance of a closed-loop system, consider an auxiliary symmetric matrix $\mathbf{Q} \in \mathbb{R}^{n_z \times n_z}$, and solve the following optimization problem,

$$\underset{\mathbf{Q},\mathbf{X},\mathbf{Y},\mathbf{A},\mathbf{B},\mathbf{C},\mathbf{D}}{\text{minimize}} \ \text{Tr}\,\mathbf{Q}$$

subject to

$$\begin{pmatrix} -\mathbf{X} & -\mathbf{I} & B_j + B\mathbf{D}F_j & A\mathbf{X} + B\mathbf{C} & A + B\mathbf{D}C \\ \star & -\mathbf{Y} & \mathbf{Y}B_j + \mathbf{B}F_j & \mathbf{A} & \mathbf{Y}A + \mathbf{B}C \\ \star & \star & -\mathbf{I} & \mathbf{0} & \mathbf{0} \\ \star & \star & \star & -\mathbf{X} & -\mathbf{I} \\ \star & \star & \star & \star & -\mathbf{Y} \end{pmatrix} \prec 0, \tag{27}$$

$$\begin{pmatrix} \mathbf{Q} & C_j\mathbf{X} + E_j\mathbf{C} & C_j + E_j\mathbf{D}C \\ \star & \mathbf{X} & \mathbf{I} \\ \star & \star & \mathbf{Y} \end{pmatrix} \succ 0. \tag{28}$$

In this work, the minimization of $\mathcal{H}_2$ performance is enforced on the complete closed-loop realization. Therefore, the first closed-loop specification is defined on the subsequent realization,

$$z^{(1)} = \begin{pmatrix} v_{sd} & v_{sq} & \omega_c \end{pmatrix}^T, \quad w^{(1)} = \begin{pmatrix} w_g^T & w_u^T & w_y^T \end{pmatrix}^T, \tag{29}$$

which implies that $L_j$ and $R_j$ are,

$$L_1 = \mathbf{I}_3, \quad R_1 = \mathbf{I}_{12}. \tag{30}$$

Even though the $\mathcal{H}_2$ performance may be suitable to counteract the effect of the measurement noise and random disturbances on the voltage $\{v_{sd}, v_{sq}\}$ and on the frequency $\omega_c$ dynamics, the microgrid model also suffers from model uncertainties and frequency-domain limitations. Therefore the $\mathcal{H}_\infty$ performance is included in the control synthesis problem. In particular, this work is interested in enforcing a $\mathcal{H}_\infty$ performance on the output-controller variable $\omega_c$ dynamic, as is presented next.

### B. Dealing With Disturbance Rejection and Frequency-Domain Specifications, $\mathcal{H}_\infty$ Performance

The model that describes the interaction between a VSC and a microgrid suffers from mainly two sources of unmodeled dynamics; (*i*) the source of high-frequency harmonics of the VSC modulation and (*ii*) the microgrid dynamic model (e.g., network model, and unbalanced or nonlinear loads). These unmodeled dynamics act as disturbances for the closed-loop system and may excite the output filter's resonance or other low-damped modes of the microgrid. These aspects can be dealt with as $\mathcal{H}_\infty$ specifications to be satisfied within the control synthesis. The LMI associated with the $\mathcal{H}_\infty$ performance is defined in the following Proposition.

*Proposition 2 ($\mathcal{H}_\infty$ Synthesis [15], [19]):* This performance index measures the input-output energy gain. The constraint

$$\|z_k^{(j)}\|_{\ell_2} < \gamma_{(j)} \|w_k^{(j)}\|_{\ell_2}, \tag{31}$$

is included as a performance index in the control synthesis problem by including the LMI (32) for the $j$-th performance specification.

$$\begin{pmatrix} -\mathbf{X} & -\mathbf{I} & \mathbf{0} & (A\mathbf{X} + B\mathbf{C}) & \mathbf{A} & \left(C_j\mathbf{X} + E_j\mathbf{C}\right) \\ \star & -\mathbf{Y} & \mathbf{0} & (A + B\mathbf{D}C) & (\mathbf{Y}A + \mathbf{B}C) & \left(C_j + E_j\mathbf{D}C\right) \\ \star & \star & -\mathbf{I}\gamma_{(j)}^2 & \left(B_j + B\mathbf{D}F_j\right) & \left(\mathbf{Y}B_j + \mathbf{B}F_j\right) & \left(D_j + E_j\mathbf{D}F_j\right) \\ \star & \star & \star & -\mathbf{X} & -\mathbf{I} & \mathbf{0} \\ \star & \star & \star & \star & -\mathbf{Y} & \mathbf{0} \\ \star & \star & \star & \star & \star & -\mathbf{I} \end{pmatrix} \prec 0 \tag{32}$$

In this work, we propose to enforce the $\mathcal{H}_\infty$ performance on different input-disturbance to output channels by limiting: (*i*) the largest singular value across the frequency-domain, and (*ii*) ensuring stability under energy-bounded grid disturbances signals. Besides, the desired performance index $\gamma_{(j)}$ in (31) is expressed as a function of the nominal current of the respective DER unit; thus, the control design procedure can be normalized.

*Remark 1:* The role of the $\mathcal{H}_\infty$ specification in the control design should not be underestimated. According to the

small-gain theorem, if the $j$-th input-disturbance to output realization satisfies the constraint (31), then one can ensure the closed-loop stability for energy-bounded disturbances not larger than $1/\gamma_{(j)}$. Hence the performance specification $\gamma_{(j)}$ specifies the degree of desired robustness under which the closed-loop system remains stable when it is subject to an $\ell_2$ disturbance.

*1) Largest Singular Value Specification Across the Frequency-Domain:* The primary controller design that governs the microgrid's transient response should consider disturbance rejection capability to the sensible modes. These modes may be related to the DER's output filter, the interaction among DER units, or the loads' dynamic response (including unbalanced and nonlinear characteristics). As these modes are unknown, it is not possible to characterize them with precision. Nevertheless, one may design the DER unit's primary controller such that the closed-loop provides disturbance rejection capability, or, in other words, ensure that the largest closed-loop singular gain through all the frequency-domain will remain below the value $\gamma$. Therefore, the $\mathcal{H}_\infty$ constraint is imposed in two different channels that characterize the effect of the disturbances at the measured output $w_y$ on the VSC frequency $\omega_c$. First, we consider that the unmodeled dynamics of the microgrid to be rejected by the closed-loop are perceived as disturbances at the output measured currents $\vec{i}_o$, or the fifth and sixth element of $w_y$, yielding to the next input to output realization

$$z^{(2)} = \omega_c, \quad w^{(2)} = \begin{pmatrix} w_{y,5} & w_{y,6} \end{pmatrix}^T, \tag{33}$$

with matrices $L_j$ and $R_j$ as,

$$L_2 = \begin{pmatrix} 0 & 0 & 1 \end{pmatrix}, \quad R_2 = \begin{pmatrix} \mathbf{0}_{2\times 10} & \mathbf{I}_2 \end{pmatrix}^T. \tag{34}$$

Second, we consider that the closed-loop performance should significantly attenuate the unmodeled dynamics perceived at the output filter; particularly, those related to the high-frequency modulation of the VSC. Therefore, the following input to output realization is considered,

$$z^{(3)} = \omega_c, \quad w^{(3)} = \begin{pmatrix} w_{y,1} & w_{y,2} & w_{y,3} & w_{y,4} \end{pmatrix}^T, \tag{35}$$

with matrices $L_j$ and $R_j$ as,

$$L_3 = \begin{pmatrix} 0 & 0 & 1 \end{pmatrix}, \quad R_3 = \begin{pmatrix} \mathbf{0}_{4\times 6} & \mathbf{I}_4 & \mathbf{0}_{4\times 2} \end{pmatrix}^T. \tag{36}$$

Hence, this work considers integrating the next two performance criteria on the control synthesis problem,

$$\left\| z^{(2)} \right\|_{\ell_2} < \gamma_{(2)} \left\| w^{(2)} \right\|_{\ell_2}, \quad \left\| z^{(3)} \right\|_{\ell_2} < \gamma_{(3)} \left\| w^{(3)} \right\|_{\ell_2}. \tag{37}$$

These specifications are enforced in the closed-loop performance by including the corresponding LMI presented in Proposition 2. It is worth noticing that, in order to counteract the microgrid disturbances, the control effort made by each DER unit should be proportional to its nominal power. However, the DER units within a microgrid are inherent to different nominal powers. Hence, in this work, the performance indexes $\gamma_{(2)}$ and $\gamma_{(3)}$ are chosen as a function of the DER unit's nominal current $i_{\mathbf{b}}$, as is presented in the numerical results in Section IV-A.

*2) Robust Stability Under Grid Disturbances:* As the synchronization of the DER units mainly determines the microgrid stability through the dynamic of the frequency $\omega_c$, this work is also interested in enforcing robust stability when it is subject to the uncertain grid disturbances in $\{v_{gd}, v_{gq}, \omega_g\}$. To that end, let us specify two additional inputs to output closed-loop channels. First, the influence of the grid voltage on the frequency dynamic can be obtained, defining

$$z^{(4)} = \omega_c, \quad w^{(4)} = \begin{pmatrix} w_{g,1} & w_{g,2} \end{pmatrix}^T, \tag{38}$$

with matrices,

$$L_4 = \left(\begin{array}{cc|c} 0 & 0 & 1 \end{array}\right), \quad R_4 = \begin{pmatrix} \mathbf{I}_2 & \mathbf{0}_{2\times 10} \end{pmatrix}^T. \tag{39}$$

Second, consider the input to output channel that describes the influence of the microgrid frequency in the DER unit frequency as,

$$z^{(5)} = \omega_c, \quad w^{(5)} = w_{g,3}, \tag{40}$$

with matrices,

$$L_5 = \left(\begin{array}{cc|c} 0 & 0 & 1 \end{array}\right), \quad R_5 = \begin{pmatrix} \mathbf{0}_{1\times 2} & 1 & \mathbf{0}_{1\times 9} \end{pmatrix}^T. \tag{41}$$

Considering that the input disturbances are energy-bounded signals, one can guarantee that the closed-loop system remains stable under an incremental disturbance gain not larger than $1/\gamma_{(j)}$ when the next criteria are included in the control synthesis problem,

$$\left\| z^{(4)} \right\|_{\ell_2} < \gamma_{(4)} \left\| w^{(4)} \right\|_{\ell_2}, \quad \left\| z^{(5)} \right\|_{\ell_2} < \gamma_{(5)} \left\| w^{(5)} \right\|_{\ell_2}. \tag{42}$$

These requirements also impose $\mathcal{H}_\infty$ constraints in the control synthesis problem. These specifications are satisfied by including the corresponding LMI in Proposition 2. The choice of $\gamma_{(j)}$ directly relates to the magnitude of the microgrid voltage and microgrid frequency, establishing a physical meaning in the control design procedure. In this work, it is considered that the microgrid voltage amplitude, $\mathbf{v}_g$, and the microgrid frequency, $\omega_g$, are represented by energy bounded signals. It means that the controller will ensure the DER unit's closed-loop stability for such bounded energy signal definitions; in Section IV-A a numerical example is provided, and the evaluation of the small-gain theorem is performed. It is also of interest to ensure a minimum decay rate time of the closed-loop, as presented next.

### C. Closed-Loop Exponential Decay Rate

The control synthesis problem can also impose an upper bound on the closed-loop exponential decay rate; hence, an additional constraint is included. The associated LMI is described next.

*Proposition 3 (Exponential Decay Rate Criterion [15], [19]):* The unforced system is said to globally exponentially converge to the origin with a decay rate faster than $\alpha$ if exists a $\eta > 0$ such that $|\mathcal{X}(t)| < \eta|\mathcal{X}(0)|e^{-\alpha t}$ $\forall t \geq 0$, where $t = k\Delta$. To include this specification in the control synthesis, the LMI (43) is included in the optimization

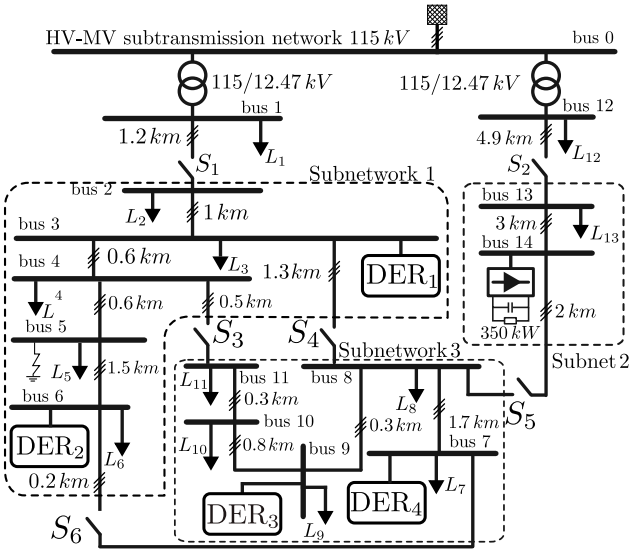


Fig. 2. CIGRE medium-voltage distribution network.

problem.

$$\begin{pmatrix} -e^{-2\alpha\Delta}\begin{pmatrix}\mathbf{X} & \mathbf{I}\\ \mathbf{I} & \mathbf{Y}\end{pmatrix} & \begin{pmatrix}A\mathbf{X}+B\mathbf{C} & A+B\mathbf{D}C\\ \mathbf{A} & \mathbf{Y}A+\mathbf{B}C\end{pmatrix}^T\\ \star & -\begin{pmatrix}\mathbf{X} & \mathbf{I}\\ \mathbf{I} & \mathbf{Y}\end{pmatrix}\end{pmatrix} \prec 0 \quad (43)$$

The above propositions complete the closed-loop specifications considered in this work.

### D. Optimization Problem

The control synthesis problem for integration of a DER unit within a microgrid system can be written as the next proposed convex optimization problem,

minimize $\mathrm{Tr}\,\mathbf{Q}$

subject to: LMIs (27) and (28) with $\{L_1, R_1\}$ in (30),
LMI (32) with $\{L_2, R_2\}$ in (34), and $\gamma_{(2)}$ chosen,
LMI (32) with $\{L_3, R_3\}$ in (36), and $\gamma_{(3)}$ chosen,
LMI (32) with $\{L_4, R_4\}$ in (39), and $\gamma_{(4)}$ chosen,
LMI (32) with $\{L_5, R_5\}$ in (41), and $\gamma_{(5)}$ chosen,
LMI (43) with $\Delta$ and $\alpha$ chosen.

A microgrid with four DER units is considered as a benchmark to assess the proposed control synthesis's effectiveness, as is presented in the next section.

## IV. Time-Domain Simulation Example

To validate the proposed control design methodology, the CIGRE medium-voltage distribution network [36] with four DER units, as is presented in Fig. 2, is simulated through the PSCAD/EMTDC software.

This microgrid presents two subnetworks, 1 and 3, that can be locally energized through their respective DER units. These subnetworks can be interconnected through the breakers $S_3$, $S_4$, and $S_6$. The subnetwork 2 is represented by a commercial load at bus 13, and a nonlinear load (rectifier with a 350 $kW$ load) at bus 14. This subnetwork can be connected to the subnetworks 1 and 3 through the breaker $S_5$. Alternatively, the microgrid can be connected to the main grid through the breakers $S_1$ and $S_2$. In order to perceive the benefits of the proposed controller in dealing with low-frequency unmodeled dynamics, the subnetworks 1 and 3 present three-phase unbalanced loads. It will be observed in the simulation results as a sustained second harmonic component in $dq$ coordinate of 120 $Hz$. Additionally, in order to test the proposed algorithm transiting to a control protection scheme, a three-phase short-circuit is simulated at bus 5. The parameters that characterize the models of the loads, distribution lines, and substation transformers are presented in [36]. The nominal values of each DER unit and the parameters that characterize the respective output filter and isolation transformer are presented in Table I. The sampling-time used for control design is the same for all DER units, $\Delta = 200\mu s$. The respective DER's power converters correspond to 2-level VSCs with a DC-link $v_{dc} = 1000\,[V]$ and a space-vector modulation strategy with period $\Delta$. The characteristics presented above serve as a simulation benchmark to validate the effectiveness of the proposed primary controller. The unbalanced three-phase loads and inter-DER dynamics represent low-frequency unmodeled dynamics. The nonlinear loads, power converters modulation and transition to protection scheme represent high-frequency unmodeled dynamics. The distribution power lines and the distribution/substation represent parameter mismatch. In order to illustrate the control synthesis for DER units, we selected DER unit 1 as a case study.

TABLE I
Nominal Values and Circuit Parameter of Each DER Unit

| Par. | $\mathrm{DER}_1$ | $\mathrm{DER}_2$ | $\mathrm{DER}_3$ | $\mathrm{DER}_4$ |
|---|---|---|---|---|
| $S_{\mathbf{b}}\,[MVA]$ | 2 | 2 | 2.5 | 1 |
| $v_{\mathbf{b}}$ | 520 [V] | | | |
| $\omega_{\mathbf{b}}$ | $2\pi 60$ [rad/s] | | | |
| $i_{\mathbf{b}}\,[kA]$ | 3.6 | 3.6 | 4.5 | 1.8 |
| $R_f\,[m\Omega]$ | 1.62 | 1.62 | 1.2 | 3.25 |
| $L_f\,[\mu H]$ | 43 | 43 | 34 | 86 |
| $C_f\,[mF]$ | 1.3 | 1.7 | 1.64 | 0.66 |
| $R_g\,[m\Omega]$ | 2 | 2 | 1.6 | 4 |
| $L_g\,[\mu H]$ | 9.3 | 9.3 | 7.4 | 1.86 |

### A. Control Synthesis Example

The control synthesis presented in this section corresponds to the implemented controller for the DER unit 1. The proposed optimization problem presented in Section III-D is solved using the interpreter CVXPY [37] and the solver CVXOPT, and the code example can be found online at [38].

In this work, we consider the specification performances $\gamma_{(j)}$ as a function of the nominal values of the respective DER unit. It permits the design of a controller that supports the microgrid disturbances in proportion to the DER unit's nominal power. The consequence of this consideration is observed in the simulation results, where all DER units respond in proportion to their nominal power during transients and steady-state conditions. Hence, for the case of the frequency-domain specifications in (37), the desired performances are chosen as $\gamma_{(2)} = \frac{2\pi}{i_{\mathbf{b}}}$ and $\gamma_{(3)} = \frac{10^{-2}}{i_{\mathbf{b}}}$. For

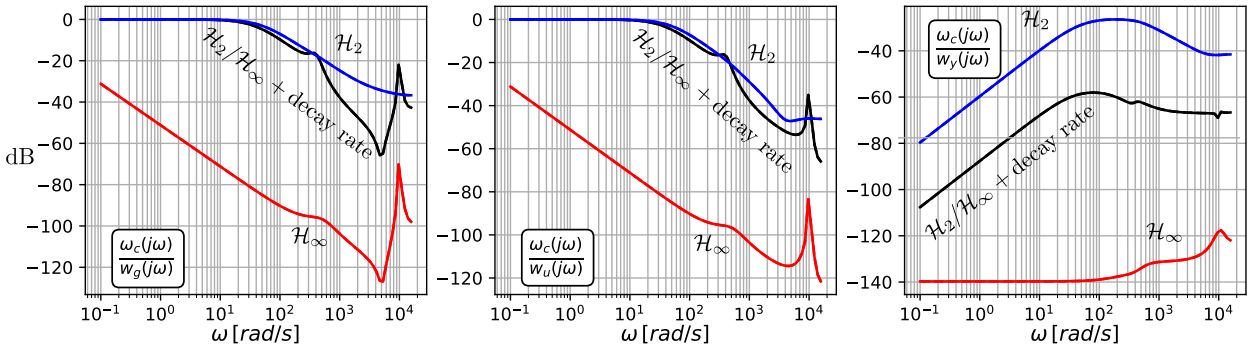


Fig. 3. Maximum singular value of the DER's frequency $\omega_c$ response under different disturbances of the closed-loop system. Left for $w_g$ grid disturbance, center for $w_u$ input disturbance, and right for $w_y$ output disturbance. In black-color the proposed controller, in blue-color the $\mathcal{H}_2$ controller and in red-color the $\mathcal{H}_\infty$ controller.

TABLE II
RESULTING CLOSED-LOOP SPECIFICATION CRITERIA $(\cdot)^*$ FOR DER 1

| | $\tau_s$ | $\gamma_{(2)}$ | $\gamma_{(3)}$ | $\gamma_{(4)}$ | $\gamma_{(5)}$ |
|---|---|---|---|---|---|
| | 0.033 | $2.45{\cdot}10^{-3}$ | $3.9{\cdot}10^{-6}$ | 52 | 6.28 |
| $\mathrm{Tr}\,\mathbf{Q}^*$ | $\tau_s^*$ | $\gamma_{(2)}^*$ | $\gamma_{(3)}^*$ | $\gamma_{(4)}^*$ | $\gamma_{(5)}^*$ |
| 39.5 | 0.028 | $1.25{\cdot}10^{-3}$ | $1.97{\cdot}10^{-6}$ | 0.15 | 1 |

grid disturbances robustness specifications in (42), the performances are chosen as $\gamma_{(4)} = 0.1v_{\mathbf{b}}$ and $\gamma_{(5)} = 2\pi$. For the closed-loop exponential decay rate in (43), in this work $\alpha$ is chosen as $\alpha = 30$, which implies that the upper bound decay rate time constant $\tau_s$ around $\tau_s = 33\,ms$.

Considering the parameters of the output filter $(R_f, L_f, C_f)$ and of the isolation transformer $(R_g, L_g)$ of the DER unit 1 in Table I, the discrete-time model (10) can be obtained by evaluating the DER-microgrid interaction model presented in Section II-A. Solving the constraint optimization problem presented in Section III-D, the decision variables $\{\mathbf{X}, \mathbf{Y}, \mathbf{A}, \mathbf{B}, \mathbf{C}, \mathbf{D}\}$ are found, and the controller (11) is obtained by performing the transformation in (21). The resulting closed-loop specifications criteria are given in the Table II.

As can be seen in Table II, all the proposed performance specifications to integrate VSC within a microgrid are met. It is worths noticing that the optimal performance specifications $\gamma_{(4)}^*$ and $\gamma_{(5)}^*$ exhibit a significant increment on the closed-loop disturbance rejection capability, respect to the original performance specifications. It means that the closed-loop system stability can be guaranteed for all perturbations $w_k^{(4)} < \gamma_{(4)} z_k^{(4)}$ and $w_k^{(5)} < \gamma_{(5)} z_k^{(5)}$, with $\gamma_{(j)}$ having incremental gain not larger than $1/\gamma_{(j)}^*$ [15]. The design of the controller for the DER units 2, 3, 4 follows an equivalent procedure. Before proceeding with the validation of this design, the resulting closed-loop system is compared with additional performance specifications in the frequency domain, and the small-gain theorem is employed to certify the closed-loop system's robustness.

### *B. Proposed $\mathcal{H}_2/\mathcal{H}_\infty$ With Decay Rate Criteria Compared With $\mathcal{H}_2$ and $\mathcal{H}_\infty$ Specifications*

The $\mathcal{H}_2$ and $\mathcal{H}_\infty$ controllers are evaluated in the frequency domain to perceive the benefits of the proposed control design procedure. To that end, the $\mathcal{H}_2$ controller is obtained by solving the optimization problem in Section III-D only considering the LMIs (27) and (28). For the $\mathcal{H}_\infty$ controller, the optimization problem in Section III-D is solved by disregarding the LMIs (27), (28) and (43). The microgrid synchronization process is mostly regulated by the frequency $\omega_c$, which is considered the most important variable. Hence, it is evaluated in the frequency-domain respect to the different disturbances of the system model; $w_g$, $w_u$ and $w_y$ (see definition in Section II-A). In Fig. 3 the maximum singular value of the resulting closed-loop systems is illustrated for each input disturbance.

As can be seen in Fig. 3, the $\mathcal{H}_2$ controller exhibits adequate attenuation to grid and input disturbances, but not to output disturbance (nonlinear loads and modulation effect). This controller yields the closed-loop dominant mode to a decay rate of $20\,ms$. On the other hand, the $\mathcal{H}_\infty$ controller exhibits excessive disturbance attenuation through all the frequency responses and a dominant mode with a decay rate of $6\,min$. The $\mathcal{H}_2/\mathcal{H}_\infty$ with decay rate, as is proposed in this work, allows to preserve the advantages on the speed of the $\mathcal{H}_2$ controller and enforce additional high-frequency disturbance attenuation through the $\mathcal{H}_\infty$ specifications. Hence, the proposed controller specifications exhibit an adequate trade-off between closed-loop speed and robustness. To confirm this improvement, time-domain simulations for different disturbances and operating points were performed for the subnetwork 1 in the islanded mode of operation. First, it is worth mentioning that the $\mathcal{H}_2$ controller was not able to reach a robust operating condition regarding the inter DER dynamics within the subnetwork 1. Second, the proposed and the $\mathcal{H}_\infty$ controllers perform similarly to load and topological changes. However, the closed-loop response under output reference disturbances $z_k$ (see definition 24) differs significantly. Output reference disturbance is perceived as an input disturbance of the closed-loop system. It corresponds to a change in the DER's operating point that may represent a desired increment or decrement on the voltage amplitude or frequency at the PoC and may be driven by a secondary controller or a local active and reactive power reference. In Figs. 4 and 5, the dynamic response of the DER units 1 and 2 for the proposed and for the $\mathcal{H}_\infty$ controllers are illustrated respectively. For both controllers at $t = 0.1\,s$ the DER unit 1 suffers an increment of $0.02\,pu$ on the voltage $v_{sd}$ and a

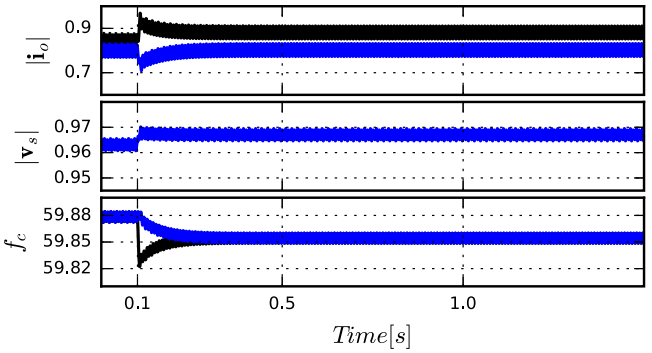


Fig. 4. Dynamic response of subnetwork 1 with proposed controller subject to an output reference disturbance. Black and blue colors represent the DERs 1 and 2, respectively.

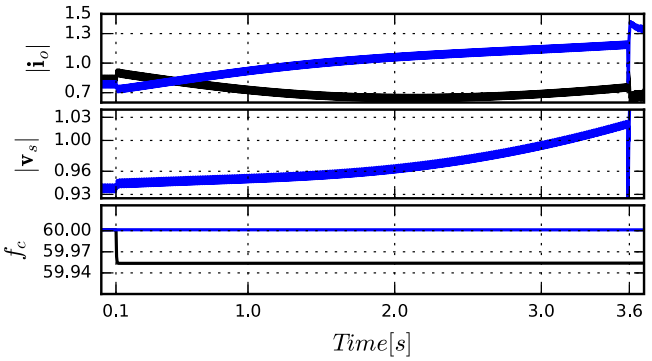


Fig. 5. Dynamic response of subnetwork 1 with $\mathcal{H}_\infty$ controller subject to an output reference disturbance. Black and blue colors represent the DERs 1 and 2, respectively.

decrement of $0.0008\,pu$ on the frequency $\omega_c$ operating points. As can be seen, the $\mathcal{H}_\infty$ controller exhibit a significant slow response, particularly for the frequency dynamic. Even though the $\mathcal{H}_\infty$ controller exhibits significant robustness properties, the synchronization dynamic-response may be slow and eventually reach desynchronization, as is perceived at $t = 3.6\,s$ in Fig. 5. It is consistent with the frequency-response mentioned above in Fig. 3 and with the resulting dominant modes. On the other hand, the benefits of the proposed controller are evidenced in Fig. 4, where the synchronization dynamic follows the expected closed-loop design.

### *C. Application of the Small-Gain Theorem to the Proposed DER's Primary Controller*

Considering the Theorem 1 presented in Section II-C, the stability condition provided by the small-gain theorem in the context of DER's integration within microgrids is evaluated as follows. Let $H_1$ be the resulting closed-loop system designed in the previous subsection. Also, let $H_2$ be the system representing the rest of the microgrid, i.e., the loads, the network, the transformers, and the other DER units. Due to the microgrid system's complexity, obtaining a system model for $H_2$ is not practical. Therefore, the small-gain theorem can be evaluated to find the maximum allowable disturbance $\ell_2$-gain such that the designed controller can ensure closed-loop stability. In this work, the voltage-amplitude and voltage-frequency stability at the DER's PoC are the output signals of interest.

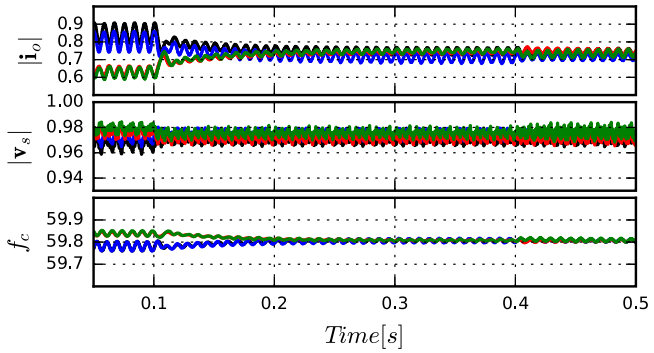


Fig. 6. Case study 1. Dynamic response of the DER units under the connection of the subnetworks 1 and 3 expressed in per-unit of each DER. Black and blue colors represent the DERs 1 and 2, red and green for DERs 3 and 4.

Due to the high microgrid model uncertainty at the PoC of each DER unit, the grid's voltage and frequency are the disturbances considered for this study. Worth noting that to find the $\ell_2$-gain of the proposed closed-loop system, the $\mathcal{H}_\infty$-norm is evaluated.

Consider the closed-loop representation in (12), (13) and evaluate the parameters of the DER unit 1 and the controller obtained in the previous subsection. Then, for the realization

$$z_k^{(6)} = \begin{bmatrix} v_{sd} & v_{sq} & \omega_c \end{bmatrix}^T, \quad w_k^{(6)} = \begin{bmatrix} v_{gd} & v_{gq} & \omega_g \end{bmatrix}^T, \quad (44)$$

one can obtain its $\mathcal{H}_\infty$-norm as,

$$\frac{\left\| z^{(6)} \right\|_{\ell_2}}{\left\| w^{(6)} \right\|_{\ell_2}} = \gamma_{(6)} = 22.16. \quad (45)$$

It means that having a disturbance $w^{(6)}$ with incremental gain not larger than $\gamma_{(6)}^{-1} = 0.045$, the stability of the interaction between the DER unit and the rest of the microgrid system is ensured.

### *D. Case Study 1: Network Topological Changes*

This case study demonstrates the DER units' dynamic responses to topological network changes. The microgrid starts in the islanded mode of operation, with the subnetworks 1 powered by the DER 1 and DER 2, and the subnetwork 3 powered by the $\text{DER}_3$ and $\text{DER}_4$. In Fig. 6, at $t = 0.1\,s$, the breaker $S_4$ is closed, connecting the subnetworks 1 and 3. Subsequently, at $t = 0.4\,s$, the breakers $S_3$ and $S_6$ are closed, changing the network topology from radial to meshed.

As aforementioned, and as can be seen in Fig. 6, the subnetworks exhibit significant load imbalance, which is perceived as an oscillation of $120\,Hz$ in the output currents $\mathbf{i}_o$. The proposed feedback law offers a significant attenuation of these currents, illustrated through the small voltage $\mathbf{v}_s$ and frequency $\omega_s$ steady-state oscillations. After closing the breaker $S_4$ at $t = 0.1\,s$, the DER units synchronize each other, following the closed-loop exponential decay rate specified in the control design ($t_s = 4\tau_s < 0.13\,s$). After the subnetworks are interconnected, the whole network's unbalance degree decreases, and the feedback law responds analogously. Also, as shown in Fig. 6, the steady-state operating point of

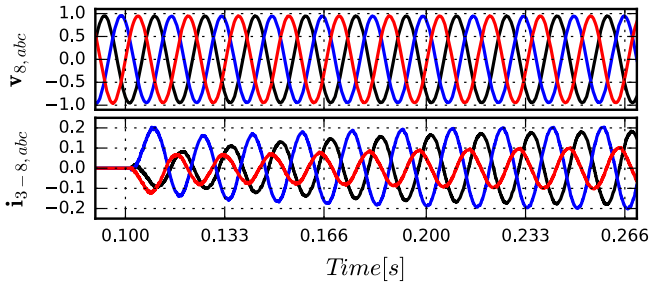


Fig. 7. Case study 1. Network dynamic response under the connection of the subnetwork 1 and 3 expressed in per-unit with microgrid base values.

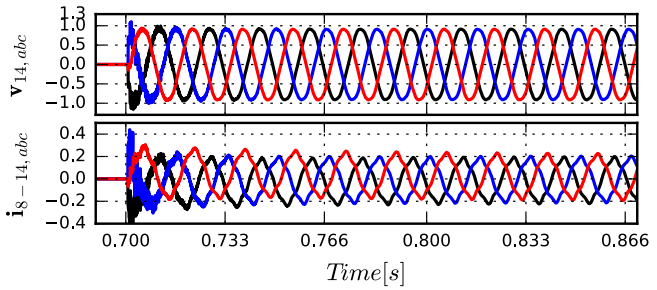


Fig. 9. Case study 2. Network dynamic response under the connection of the subnetwork 2 expressed in per-unit with microgrid base values.

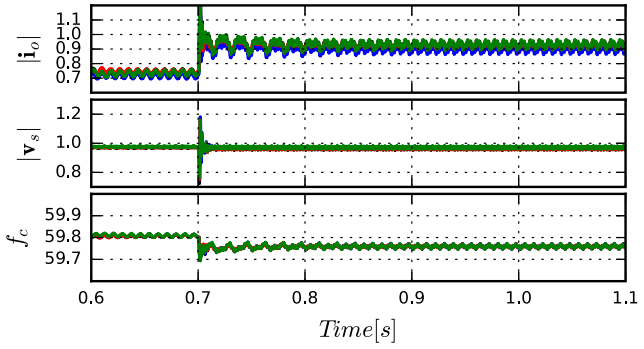


Fig. 8. Case study 2. Dynamic response of the DER units under the connection of the subnetwork 2 expressed in per-unit of each DER. Black and blue colors represent the DERs 1 and 2, red and green for DERs 3 and 4.

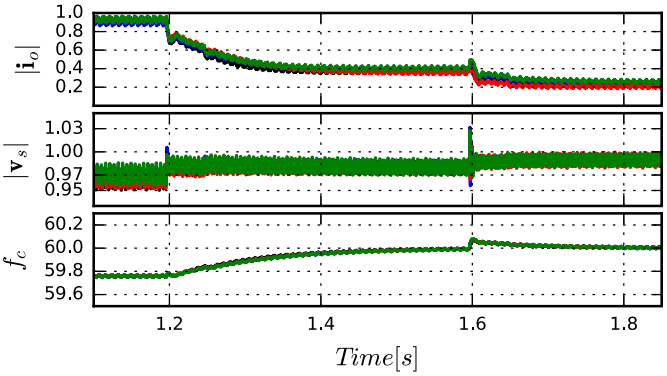


Fig. 10. Case study 3. Dynamic response of the DER units during a transition to grid-connected mode, expressed in per-unit of each DER. Black and blue colors represent the DERs 1 and 2, red and green for DERs 3 and 4.

the respective DER units' currents are closely proportional to their nominal powers, offering power-sharing capability. Also, Fig. 7 illustrates the network's dynamic response in *abc* coordinate at bus 8.

### *E. Case Study 2: Nonlinear Load Connection*

This case study exhibits the DER units' dynamic response to the connection of the subnetwork 2. In particular, this case study shows the DER units' capability to support a black-start and the controller's ability to attenuate the high-frequency distortion produced by the rectifier on the voltage and frequency of the microgrid. In Figs. 8 and 9, the microgrid is initially at the same steady-state at the end of the Case 1. At $t = 0.7\,s$ the breaker $S_5$ is closed, and the subnetwork 2 is powered by the DER units of the subnetworks 1 and 3. This event can be interpreted as a disturbance for the DERs' closed-loop system, which produces a significant drop in the voltage $\mathbf{v}_g$. In order to recover the voltage of the microgrid, the DER units deliver a significant amount of current while the subnetwork 2 achieves its voltage condition, as can be seen in Fig. 9.

Once the voltage and current of the subnetwork 2 reach its steady-state condition, the rectifier's impact is perceived as high-frequency harmonic content in its demanded currents, as is seen in Fig. 9. The effect of this harmonic content in *dq* coordinates is about 10% of each DER's nominal current, see Fig. 8. The closed-loop system can attenuate this disturbance, offering a distortion of about 3% on the microgrid voltage and distortion of about 0.05% on the microgrid frequency, with respect to their nominal values. It is also worth noting that, as the controllers were designed following performance specifications regarding the DER's nominal power, the harmonic content is approximately shared between DER units.

### *F. Case Study 3: Microgrid Transition To Grid-Connected Mode*

This case study exhibits the DER units' dynamic response during the microgrid transition to the grid-connected operation mode. This change in the mode of operation represents an abrupt change in the network's voltage and frequency model; in grid-connected mode, $\mathbf{v}_g$ and $\omega_g$ are principally regulated by the main grid. It means that the microgrid model's uncertainties are now mostly perceived in the synchronization process rather than in the microgrid voltage and frequency dynamic. Therefore, this case study illustrates the benefits of the proposed closed-loop design in handling these disturbances. Initially, the microgrid is at the same steady-state at the end of Case 2; the microgrid is in the islanded mode of operation and powering all the subnetworks. In Figs. 10 and 11, at $t = 1.2\,s$ the breaker $S_1$ is closed, and the microgrid transits to the grid-connected mode of operation. Subsequently, at $t = 1.6\,s$ the breaker $S_2$ is closed. As shown in Fig. 10, the DER units exhibit a smooth dynamic response during the transition. The voltage's dynamic response effectively counteracts this disturbance, while the frequency and the current converge to the steady-state in approximately $0.3\,s$, without oscillations. The discrepancy between the designed closed-loop dominant mode ($t_s < 0.13\,s$) and the obtained from the simulation is mainly caused by the parametric errors that arise from the

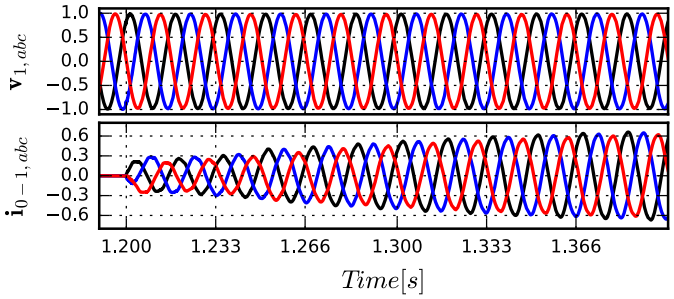


Fig. 11. Case study 3. Network dynamic response during the transition to grid-connected mode expressed in per-unit with microgrid base values.

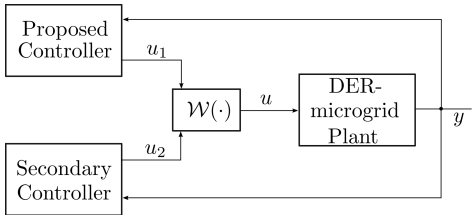


Fig. 12. Case study 4. Control structure employed for limiting the power converter output current.

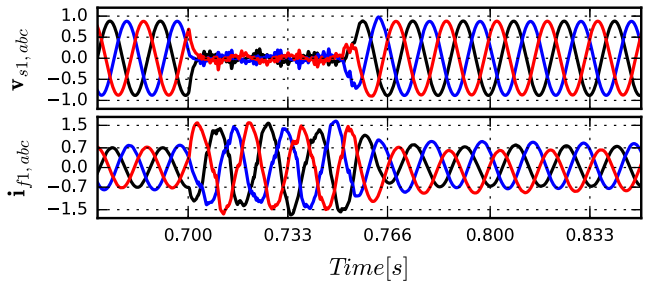


Fig. 13. Case study 4. DER unit 1 dynamic response during three-phase short circuit.

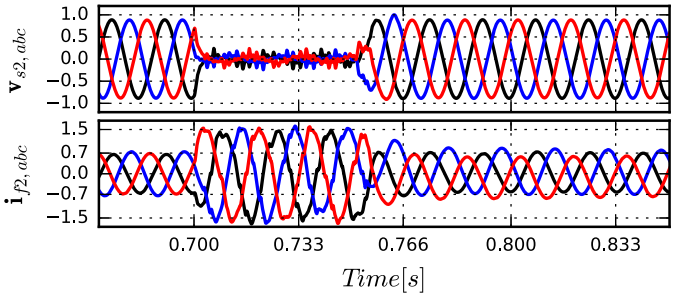


Fig. 14. Case study 4. DER unit 2 dynamic response during three-phase short circuit.

substations reactance transformers ($X/R \approx 10$). It confirms that the proposed control design can provide robustness under uncertain parameters, in particular for those related to the distribution transformers at the microgrid's substation. The dynamic response at the bus where the microgrid is connected is also depicted in *abc* coordinates in Fig. 11.

It is worth noticing that the main grid supplies part of the harmonic components required by the network and loads (unbalanced and nonlinear), and the DER units cooperate in supplying such requirements. Also, as can be seen in Fig. 10, the DER units preserve their power-sharing capability in grid-connected mode.

### G. Case Study 4: Three-Phase Short-Circuit Disturbance

This case scenario tests the proposed DER units' controller when the microgrid system is subject to a short-circuit disturbance. Under this incident, the controller of each DER unit should maintain its electrical connection to the microgrid and protect the power conversion system against excessive overcurrent while the fault is cleared. To overcome these requirements, the controller should prioritize the current over the voltage regulation, resulting in a change of the closed-loop control objective. It means that the controller is required to maintain limits on the inverter current $\mathbf{i}_f$ at high bandwidth to avoid undesirable transient phenomena. This transition on the control objective is perceived as a switching closed-loop structure such that the proposed controller should stabilize. Hence, in this Case study, the effectiveness of the proposed controller is evaluated in a time-domain simulation during an objective control transition. To that end, the switching controller is carried out as presented in [39], and schematized in Fig. 12.

In this figure, the secondary controller represents a conventional regulation law of the output converter current, as is presented in [40], and in the current work, it is designed for a bandwidth of $600\frac{rad}{s}$. For the switching strategy $\mathcal{W}(\cdot)$, the following algorithm is implemented,

$$u = \lambda u_2 + (1-\lambda)u_1 \tag{46}$$

with $\lambda$ as,

$$\lambda = \begin{cases} 0, & \text{for } |y| \leq y_l \\ \frac{|y|-y_l}{y_h-y_l}, & \text{for } y_h > |y| > y_l \\ 1, & \text{for } |y| \geq y_h, \end{cases} \tag{47}$$

where $y_h$ and $y_l$ are the desired boundary of the current limitation; in this work $y_l = 1.25\,pu$ and $y_h = 1.5\,pu$ for the direct ($i_{fd}$) and quadrature ($i_{fq}$) currents of each DER unit. In order to observe the proposed controller ability of handling the transition from/to this current structure limitation, a three-phase short-circuit strikes the subnetwork 1 at bus 5, while it operates in islanded mode. The dynamic response of the DER units 1 and 2 is illustrated in Figs. 13 and 14, respectively, where the short-circuit lasts $50\,ms$.

From Figs. 13 and 14 it can be observed that the proposed controller can effectively deal with the transition to current regulation during short-circuit disturbance within the microgrid system.

## V. Conclusion

This paper has proposed a control design methodology for the decentralized integration of DER units in AC microgrid systems. This methodology is based on a convex optimization problem subject to matrix inequalities, and it provides a linear dynamic output-feedback controller that guarantees closed-loop stability and performance specifications. In particular,

this work suggests the minimization of the $\mathcal{H}_2$ performance subject to $\mathcal{H}_\infty$ specifications on particular input to output closed-loop channels. While the $\mathcal{H}_2$ performance is imposed to deal with stochastic aspects and random disturbances, the $\mathcal{H}_\infty$ is considered to enforce robustness to model uncertainties of the DER-microgrid interaction model. The small-gain theorem is used to provide the degree of robustness of the resulting closed-loop system. The simulation results show that the DER units perform according to the specified design in the islanded mode for a network that exhibits unbalanced and nonlinear loads. In grid-connected, the main grid's parameter mismatch results in a slower microgrid primary response; nevertheless, it still offers a stable operation, even during its transition. Hence, this work concludes that the proposed control design methodology and performance specifications provide a powerful tool to improve DER units' robustness operating in microgrid systems.

## REFERENCES


[1] S. Parhizi, H. Lotfi, A. Khodaei, and S. Bahramirad, "State of the art in research on microgrids: A review," *IEEE Access*, vol. 3, pp. 890–925, 2015.

[2] *IEEE Standard for the Specification of Microgrid Controllers*, IEEE Standard 2030.7-2017, pp. 1–43, 2018.

[3] M. Farrokhabadi *et al.*, "Microgrid stability definitions, analysis, and examples," *IEEE Trans. Power Syst.*, vol. 35, no. 1, pp. 13–29, Jan. 2020.

[4] J. Schiffer, R. Ortega, A. Astolfi, J. Raisch, and T. Sezi, "Conditions for stability of droop-controlled inverter-based microgrids," *Automatica*, vol. 50, no. 10, pp. 2457–2469, 2014.

[5] J. W. Simpson-Porco, F. Dörfler, and F. Bullo, "Synchronization and power sharing for droop-controlled inverters in islanded microgrids," *Automatica*, vol. 49, no. 9, pp. 2603–2611, 2013.

[6] J. W. Simpson-Porco, F. Dörfler, and F. Bullo, "Voltage stabilization in microgrids via quadratic droop control," *IEEE Trans. Autom. Control*, vol. 62, no. 3, pp. 1239–1253, Mar. 2017.

[7] M. J. Hossain, H. R. Pota, M. A. Mahmud, and M. Aldeen, "Robust control for power sharing in microgrids with low-inertia wind and PV generators," *IEEE Trans. Sustain. Energy*, vol. 6, no. 3, pp. 1067–1077, Jul. 2015.

[8] S. S. Madani, C. Kammer, and A. Karimi, "Data-driven distributed combined primary and secondary control in microgrids," *IEEE Trans. Control Syst. Technol.*, vol. 29, no. 3, pp. 1340–1347, May 2021.

[9] H. Bevrani, M. R. Feizi, and S. Ataee, "Robust frequency control in an islanded microgrid: $H_\infty$ and $\mu$ -synthesis approaches," *IEEE Trans. Smart Grid*, vol. 7, no. 2, pp. 706–717, Mar. 2016.

[10] S. M. Hoseinizadeh, S. Ouni, H. Karimi, M. Karimi-Ghartemani, and K. L. Lian, "Comparison of PLL-based and PLL-less vector current controllers," *IEEE J. Emerg. Sel. Topics Power Electron.*, early access, Mar. 17, 2021, doi: 10.1109/JESTPE.2021.3066512.

[11] M. Ashabani, Y. A. R. I. Mohamed, M. Mirsalim, and M. Aghashabani, "Multivariable droop control of synchronous current converters in weak grids/microgrids with decoupled *dq*-axes currents," *IEEE Trans. Smart Grid*, vol. 6, no. 4, pp. 1610–1620, Jul. 2015.

[12] Q. Zhong, G. C. Konstantopoulos, B. Ren, and M. Krstic, "Improved synchronverters with bounded frequency and voltage for smart grid integration," *IEEE Trans. Smart Grid*, vol. 9, no. 2, pp. 786–796, Mar. 2018.

[13] R. Pérez-Ibacache, C. A. Silva, and A. Yazdani, "Linear state-feedback primary control for enhanced dynamic response of AC microgrids," *IEEE Trans. Smart Grid*, vol. 10, no. 3, pp. 3149–3161, May 2019.

[14] K. R. Vasudevan, V. K. Ramachandaramurthy, T. S. Babu, and A. Pouryekta, "Synchronverter: A comprehensive review of modifications, stability assessment, applications and future perspectives," *IEEE Access*, vol. 8, pp. 131565–131589, 2020.

[15] C. Scherer, P. Gahinet, and M. Chilali, "Multiobjective output-feedback control via LMI optimization," *IEEE Tran. Autom. Control*, vol. 42, no. 7, pp. 896–911, Jul. 1997.

[16] L. Ravanbod, D. Noll, and P. Apkarian, "An extension of the linear quadratic gaussian-loop transfer recovery procedure," *IET Control Theory Appl.*, vol. 6, no. 14, pp. 2269–2278, 2012.

[17] S. Boyd, L. El Ghaoui, E. Feron, and V. Balakrishnan, *Linear Matrix Inequalities in System and Control Theory*, vol. 15. Philadelphia, PA, USA: SIAM, Jun. 1994.

[18] M. A. Rami and X. Y. Zhou, "Linear matrix inequalities, Riccati equations, and indefinite stochastic linear quadratic controls," *IEEE Trans. Autom. Control*, vol. 45, no. 6, pp. 1131–1143, Jun. 2000.

[19] D. Grigoriadis, *A Unified Algebraic Approach To Control Design,* 1st ed. Milton, U.K.: Routledge, 1998. [Online]. Available: https://doi.org/10.1201/9781315136523

[20] S. Boyd and L. Vandenberghe, *Convex Optimization*. Cambridge, U.K.: Cambridge Univ. Press, 2004.

[21] I. J. Gabe, V. F. Montagner, and H. Pinheiro, "Design and implementation of a robust current controller for VSI connected to the grid through an LCL filter," *IEEE Trans. Power Electron.*, vol. 24, no. 6, pp. 1444–1452, Jun. 2009.

[22] M. Babazadeh and H. Karimi, "A robust two-degree-of-freedom control strategy for an islanded microgrid," *IEEE Trans. Power Del.*, vol. 28, no. 3, pp. 1339–1347, Jul. 2013.

[23] P. Buduma and G. Panda, "LQR based control method for grid connected and islanded DG system," *Int. J. Emerg. Elect. Power Syst.*, vol. 19, no. 5, Oct. 2018, Art. no. 20180027.

[24] M. Armin, P. N. Roy, S. K. Sarkar, and S. K. Das, "LMI-based robust PID controller design for voltage control of islanded microgrid," *Asian J. Control*, vol. 20, no. 5, pp. 2014–2025, 2018.

[25] H. R. Baghaee, M. Mirsalim, G. B. Gharehpetian, and H. A. Talebi, "A decentralized robust Mixed $\mathcal{H}_2/\mathcal{H}_\infty$ voltage control scheme to improve small/large-signal stability and FRT capability of islanded multi-DER microgrid considering load disturbances," *IEEE Syst. J.*, vol. 12, no. 3, pp. 2610–2621, Sep. 2018.

[26] G. G. Koch, L. A. Maccari, R. C. L. F. Oliveira, and V. F. Montagner, "Robust $\mathcal{H}_\infty$ state feedback controllers based on linear matrix inequalities applied to grid-connected converters," *IEEE Trans. Ind. Electron.*, vol. 66, no. 8, pp. 6021–6031, Aug. 2019.

[27] M. Armin *et al.*, "Robust extended $\mathcal{H}_\infty$ control strategy using linear matrix inequality approach for islanded microgrid," *IEEE Access*, vol. 8, pp. 135883–135896, 2020.

[28] M. Raeispour, H. Atrianfar, H. R. Baghaee, and G. B. Gharehpetian, "Robust sliding mode and mixed $H_2/H_\infty$ output feedback primary control of AC microgrids," *IEEE Syst. J.*, vol. 15, no. 2, pp. 2420–2431, Jun. 2021.

[29] L. Huang, H. Xin, and F. Dörfler, "H∞-control of grid-connected converters: Design, objectives and decentralized stability certificates," *IEEE Trans. Smart Grid*, vol. 11, no. 5, pp. 3805–3816, Sep. 2020.

[30] R. K. Sharma, S. Mishra, and D. Pullaguram, "A robust $H_\infty$ multivariable stabilizer design for droop based autonomous ac microgrid," *IEEE Trans. Power Syst.*, vol. 35, no. 6, pp. 4369–4382, Nov. 2020.

[31] A. Fathi, Q. Shafiee, and H. Bevrani, "Robust frequency control of microgrids using an extended virtual synchronous generator," *IEEE Trans. Power Syst.*, vol. 33, no. 6, pp. 6289–6297, Nov. 2018.

[32] N. Pogaku, M. Prodanovic, and T. C. Green, "Modeling, analysis and testing of autonomous operation of an inverter-based microgrid," *IEEE Trans. Power Electron.*, vol. 22, no. 2, pp. 613–625, Mar. 2007.

[33] R. A. DeCarlo, *Linear Systems: A State Variable Approach With Numerical Implementation*. Englewood Cliffs, NJ, USA: Prentice-Hall, 1989.

[34] I. Masubuchi, A. Ohara, and N. Suda, "LMI-based controller synthesis: A unified formulation and solution," *Int. J. Robust Nonlinear Control*, vol. 8, no. 8, pp. 669–686, 1998.

[35] H. K. Khalil, *Nonlinear Systems*, 3rd ed. Upper Saddle River, NJ, USA: Prentice-Hall, 2002.

[36] *Benchmark Systems for Network Integration of Renewable and Distributed Energy Resources*, CIGRE, Paris, France, 2014.

[37] S. Diamond and S. Boyd, "CVXPY: A Python-embedded modeling language for convex optimization," *J. Mach. Learn. Res.*, vol. 17, no. 83, pp. 1–5, 2016.

[38] R. R. Perez-Ibacache, R. da Silveira Castro, G. A. Pimentel, and B. S. Bizzo. "LMI_Control_DER_Units." 2020. [Online]. Available: https://github.com/rperezibacache/LMI_Control_DER_units.git

[39] G. C. Goodwin, S. F. Graebe, and M. E. Salgado, *Control System Design*, 1st ed. Upper Saddle River, NJ, USA: Prentice-Hall, 2000, pp. 291–306.

[40] A. Yazdani and R. Iravani, *Voltage-Sourced Converters in Power Systems: Modeling, Control, and Applications*. Hoboken, NJ, USA: Wiley, 2010, pp. 204–244.

**Ricardo Pérez-Ibacache** received the B.Eng., M.Sc.Eng., and Dr.Eng. degrees in electronic engineering from the Universidad Técnica Federico Santa María, Valparaíso, Chile, in 2012 and 2018, respectively. In 2014 and 2016, he was a visiting Ph.D. student with the University of Ryerson, Toronto, ON, Canada, conducting modeling and control design research for distributed energy resources. From 2018 to 2020, he was a Postdoctoral Researcher with the Grupo de Automação e Controle de Sistemas, PUCRS, Porto Alegre, Brazil. He is currently with Andes Volt Industrial, Valdivia, Chile. He is involved in designing and manufacturing power electronic systems, control design for integrating DERs in low and medium voltage distribution networks, and SoC design and development. His main interests include power electronics, microgrid systems, and control engineering.

**Rafael S. Castro** received the bachelor's degree in automation and control engineering from Pontifical Catholic University of Rio Grande do Sul (PUCRS), Brazil, in 2013, where he earned an accolade for outstanding academic achievement, the M.S. degree in electrical engineering from PUCRS in 2015, and the Ph.D. degree in electrical engineering from the Federal University of Rio Grande do Sul (UFRGS), in 2019, in the subarea of automation and control. He is currently an Associate Professor and a Researcher with the PUCRS. His research interests include robust control and output regulation of nonlinear systems, with several published papers in the field.

**Guilherme Araujo Pimentel** received the B.Eng. degree in control and automation and the M.Sc. degree in electrical engineering from the Pontifical Catholic University of Rio Grande do Sul, Brazil, in 2007 and 2010, respectively, and the joint Ph.D. degree in science of engineering from the University of Mons, Belgium, and in mathematics and modeling from the University of Montpellier, France, in 2015. From 2015 to 2017, he had a postdoctoral position with the Department of Automation and Energy, Universidade Federal do Rio Grande do Sul, Porto Alegre, Brazil. From August 2015 ro January 2021, he was an Associate Professor with the School of Technology, Pontifical Catholic University of Rio Grande do Sul (PUCRS). Since February 2021, he has a researcher position with SECO Group. His main research interests are system identification, modeling, and control of (non)linear systems.

**Bruno Salgado Bizzo** received the B.Eng. degree in electronic engineering from the Military Institute of Engineering, Brazil, in 2003. He is currently pursuing the M.Sc.Eng. degree with Pontifical Catholic University of Rio Grande do Sul, Brazil. His main research interests focus on applied control theory.